J. Fluid Mech. (2015), *vol.* 778, R5, doi:10.1017/jfm.2015.433

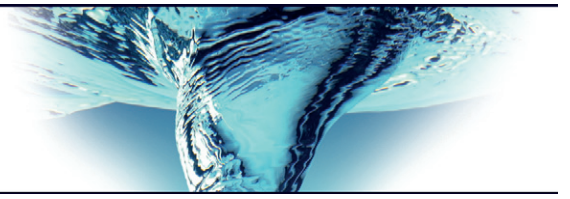

Reversals of the large-scale circulation in quasi-2D Rayleigh–Bénard convection

Rui Ni[1],‡, **Shi-Di Huang**[1] **and Ke-Qing Xia**[1],†

[1]Department of Physics, The Chinese University of Hong Kong, Shatin, Hong Kong, China

(Received 10 June 2015; revised 17 July 2015; accepted 22 July 2015;
first published online 4 August 2015)

We report an experimental study of the large-scale circulation (LSC) reversal in quasi-2D turbulent thermal convection, in which the aspect ratio Γ (= height/length of a rectangular box) is used as a parameter to perturb the stability of the LSC. It is found that the mean time interval $\langle\tau\rangle$ between two successive reversals increases strongly with increasing Γ. A stochastic model is proposed to incorporate the effect of the corner rolls. In the model, the aspect ratio serves as a tuning parameter for the relative weight of the corner rolls that damp the LSC. The model predictions for the shape of the bistable states of the system and $\langle\tau\rangle$ agree excellently with the experimental results, with $\langle\tau\rangle$ having an unexpected stretched exponential Rayleigh number dependence, $\sim\exp(Ra^{\alpha})$. We further show quantitatively that the main damping force of the LSC in a quasi-2D system is from the corner rolls rather than the viscous drag from the sidewalls, which bridges the difference found in quasi-2D and 3D systems.

Key words: Bénard convection, plumes/thermals, turbulent convection

1. Introduction

Turbulent Rayleigh–Bénard (RB) convection in a fluid heated from below and cooled from above has been a subject of longstanding interest and has many applications in science and engineering (Ahlers, Grossmann & Lohse 2009; Lohse & Xia 2010; Chillà & Schumacher 2012; Xia 2013). A salient feature of turbulent RB convection is a large-scale circulation (LSC) superimposed on the turbulent background. The LSC in three-dimensional (3D) cylindrical cells of aspect ratio around one has a quasi-2D single-roll structure with a finite width of approximately half the cell diameter (Xi, Zhou & Xia 2006). Driven by the small-scale turbulent fluctuations, the vertical circulating plane of the LSC has an incessant azimuthal

† Email address for correspondence: kxia@phy.cuhk.edu.hk
‡ Present address: Department of Mechanical and Nuclear Engineering, Pennsylvania State University, State College, PA 16802-1412, USA.

meandering in this particular geometry (Cioni, Ciliberto & Sommeria 1997; Brown, Nikolaenko & Ahlers 2005; Sun, Xi & Xia 2005; Xi *et al.* 2006). In addition, the LSC sometimes stops and restarts in a different direction, termed cessation. When the new direction is opposite to the one before cessation, this event is called reversal (Cioni *et al.* 1997; Brown *et al.* 2005; Tsuji *et al.* 2005; Xi *et al.* 2006; Xi & Xia 2007), which has also been observed in the magnetic polarity of the Earth (Glatzmaier *et al.* 1999) and in the wind direction in the Earth's atmosphere (van Doorn *et al.* 2000).

The observed reversal phenomenon of the LSC has prompted several models based on either stochastic differential equations (Sreenivasan, Bershadskii & Niemela 2002; Benzi 2005) or deterministic ones (Araujo, Grossmann & Lohse 2005). All of these 2D models are able to produce switchings between two bistable states. However, as they are not derived from the equations of motion, it is not possible for them to make quantitative comparisons between model predictions and experimentally measured quantities. Motivated by this, Brown & Ahlers (2007, 2008) proposed a deterministic model consisting of two coupled stochastic ordinary differential equations that were able to produce some of the important features of the LSC in 3D RB convection, such as cessations and the azimuthal meandering. Later, Assaf, Angheluta & Goldenfeld (2011) improved the model by including the diffusion effect in the equation.

A common feature in all of the previous models is the assumption, either explicitly or implicitly, that the cessations (and reversals) of the LSC are largely independent of its azimuthal orientational dynamics. An intuitive expectation would be that if one confines the LSC into a 2D or quasi-2D convection cell, the geometry will limit the azimuthal position of the LSC plane, and with the removal of the complicated 3D dynamics, some essential features of the reversal dynamics may be revealed. Motivated by this, Sugiyama *et al.* (2010) made a combined experimental and numerical study of LSC reversals in the 2D/quasi-2D system, which covered a wide region of the *Ra*–*Pr* phase space (*Ra*: Rayleigh number; *Pr*: Prandtl number. Their exact definitions can be found in § 2). Their study revealed the key role played by the corner rolls in triggering reversal events and found an important difference between the 2D/quasi-2D and the 3D geometries, i.e. the mean time between successive reversals has a strong *Ra* dependence in the former and is essentially *Ra*-independent in the latter (Brown & Ahlers 2006; Xi & Xia 2007). The importance of the corner rolls was also found later by a number of numerical and experimental studies in the 2D/quasi-2D system (Chandra & Verma 2011, 2013; Vasilev & Frick 2011; Yanagisawa *et al.* 2011; Wagner & Shishkina 2013). As the dynamics of flow reversals appears to have quite different dimensional dependence, the question then is whether flow reversals in the RB system in the 2D and 3D cases can be described by a unified framework. A related question would be how to quantify the role played by the corner rolls.

In this paper, we report an experimental study of flow reversals in a quasi-2D geometry. We use the aspect ratio Γ (= height/length of the vertical plane in a rectangular box) as a tuning parameter for the weight of the corner rolls relative to that of the LSC. It should be noted that in Sugiyama *et al.* (2010) it was already found that Γ has a strong effect on the flow dynamics, but no quantitative and systematic study on the effect of Γ was made. The remainder of the paper is organized as follows. In § 2, we give a brief discussion of the experimental methods and the algorithm used to extract the reversal events. In § 3, we present the statistics of the time intervals between successive reversals and its dependence on the Rayleigh number and aspect ratio. We explain our experimental observations by extending the model of Brown & Ahlers (2007, 2008) to include the effects of corner rolls and

thermal diffusion through thermal plumes. Our model not only accurately reproduces the experimental findings, but may also be used to bridge the differences between 2D and 3D systems.

2. Methods

It is known that the reversal dynamics is very sensitive to the aspect ratio Γ in 3D (Xi & Xia 2007) and in 2D/quasi-2D (Sugiyama *et al.* 2010). In this study we use Γ as a parameter to perturb the stability of the LSC and also test our proposed model. Six convection cells are used, which are vertical rectangular boxes with top and bottom copper plates and plexiglas sidewalls (Xia, Sun & Zhou 2003). They have the same horizontal cross-section of 126.0 $(L) \times 38.0\,(W)$ (mm^2), but have heights H (mm) of 150.0, 140.8, 131.4, 126.3, 121.0 and 114.6. The corresponding aspect ratios $\Gamma = H/L$ are thus 0.84, 0.89, 0.96, 1.00, 1.04 and 1.10. All experiments are conducted at the same Prandtl numbers $Pr\,(= \nu/\kappa) = 5.7$, with the Rayleigh number $Ra\,(= \alpha g \Delta T H^3/\nu\kappa)$ spanning from 10^8 to 2×10^9. Here, ΔT is the temperature difference across the fluid layer, g is the gravitational acceleration, and α, ν and κ are the thermal expansion coefficient, kinematic viscosity and thermal diffusivity of water respectively. With the rectangular geometry, the large-scale flow is expected to be largely confined in the vertical LH plane (Xia *et al.* 2003). During a reversal process, the hot rising and cold falling plumes will switch their positions, causing the temperature change in the left and right sides of the plate. This allows us to use their contrast $\Delta_{bot} = T_{bot,right} - T_{bot,left}$ as a measure of reversals of the LSC (Sugiyama *et al.* 2010), where $T_{bot,right}$ and $T_{bot,left}$ are the temperatures measured by the thermistors embedded inside the bottom plate: $\sim$2 mm away from the fluid–copper interface, $W/2$ from the long edges and $L/4$ away from its right and left edges respectively. The typical value of the ratio $\Delta_{bot}/\Delta T$ is approximately 0.05.

3. Results and discussion

Figure 1 shows typical time series of Δ_{bot} for four values of Ra ranging from 4.27×10^8 to 2.38×10^9 in the $\Gamma = 0.89$ cell. In the plot, Δ_{bot} is normalized by the standard deviation σ of Δ_{bot} for either flow direction and the time t is normalized by the LSC turnover time $t_E = (2H + 2L)/U$, where U is the typical velocity of the LSC measured at $\sim H/10$ from the sidewalls and plates in a similar set-up using laser Doppler velocimetry (Xia, Zhou & Sun 2005). It is seen that there are several events with abrupt changes of temperature for all four examples shown here, and the frequency of reversal seems to increase with decreasing Rayleigh number. To quantitatively discuss the reversal frequency, we define the start (t_s) and end (t_e) times of one reversal event as the respective time instant when Δ_{bot} departs from one state and reaches the other one. Three reversals determined in this way are marked by the red circles (t_s) and blue triangles (t_e) in figure 1(*a*). We further define the time interval between two successive reversals n and $n+1$ as $\tau = t_s(n+1) - t_e(n)$, using the criterion that after each reversal the flow must persist in the new direction for at least one LSC turnover time t_E. The bistable behaviour of the LSC can also be seen from the probability density function (PDF) of Δ_{bot}/σ shown in figure 2. The Ra dependence of the normalized mean time interval between successive reversals $\langle\tau\rangle/t_E$ for different values of Γ is shown in figure 3. It is seen that there is a strong Ra dependence of the mean time interval for all values of Γ, and the dependence, surprisingly, cannot be explained by a simple power-law relationship. Moreover,

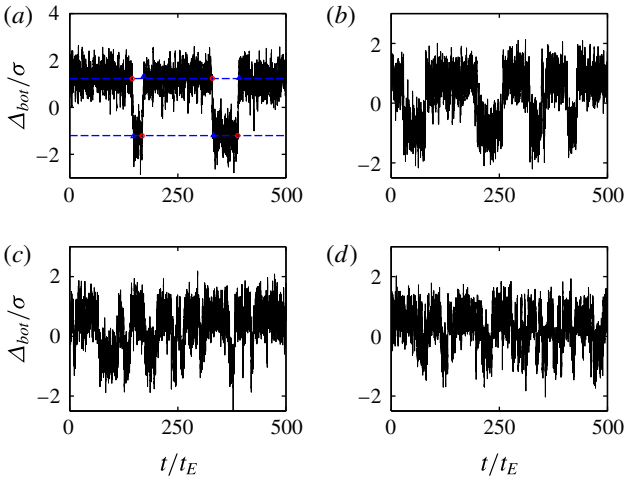

FIGURE 1. Time series of the normalized bottom plate temperature difference Δ_{bot}/σ for four Rayleigh numbers, (*a*) 2.38×10^9, (*b*) 1.02×10^9, (*c*) 6.55×10^8, (*d*) 4.27×10^8, in $\Gamma = 0.89$. The red circles and blue triangles in (*a*) are respectively reversal start points and end points determined by using the criterion described in the text.

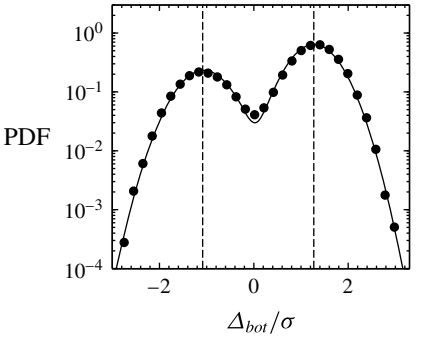

FIGURE 2. The PDF of the normalized LSC amplitude Δ_{bot}/σ ($Ra = 2.38 \times 10^9$, $\Gamma = 0.89$). The solid line is the fitting result using the sum of two independent Gaussian functions. The two dashed lines show the most probable states corresponding to the two circulation directions of the LSC.

unlike the aspect ratio dependence of the Reynolds number (Lam *et al.* 2002), there is no simple function of Γ that can collapse all curves.

The stochastic model proposed by Brown and Ahlers can explain the experimental results well in a three-dimensional cylindrical cell (Brown & Ahlers 2007, 2008). The model is motivated from the physically relevant terms in the Navier–Stokes equation for the Rayleigh–Bénard convection (Brown & Ahlers 2008). This model predicts a skewed PDF of the LSC amplitude that favours a small LSC amplitude (Brown & Ahlers 2008), which is very different from the Gaussian distribution of Δ_{bot} for the quasi-2D case as shown in figure 2. This is another feature that differentiates 3D from 2D/quasi-2D cases, apart from that of the mean time between successive reversals (or reversal frequency). We now extend the Brown–Ahlers model to explain the reversal behaviour of the LSC in quasi-2D geometry. Following the same procedure as that in

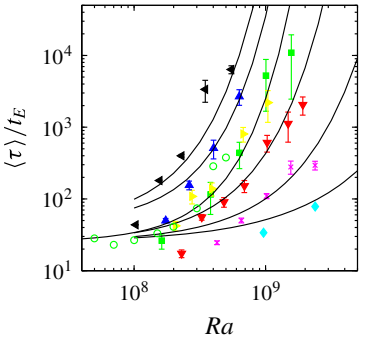

FIGURE 3. The Rayleigh number dependence of the normalized mean time interval between two successive reversals $\langle\tau\rangle$. From left to right, the symbols represent $\Gamma = 1.10$ (black left-pointing triangle), 1.04 (blue triangle), 1.00 (two independent measurements, yellow right-pointing triangles and green squares), 1.00 (green circles, simulation data from Sugiyama *et al.* (2010)), 0.96 (red down-pointing triangle), 0.89 (magenta crosses), 0.84 (cyan diamonds). See the text for the explanation of the solid lines.

Brown & Ahlers (2007) and using δ, the absolute value of Δ_{bot}, for the LSC strength, we derived the Langevin equation for the 2D geometry and found it to be

$$\dot{\delta} = \frac{\delta}{\tau_\delta} - \frac{\delta^{3/2}}{\tau_\delta\sqrt{\delta_0}} + f_\delta(t), \tag{3.1}$$

where $\tau_\delta = H^2/(108\nu Re^{1/2})$ and $\delta_0 = 216Re^{3/2}\nu^2/(\alpha g H^3)$. We also note that (3.1) is the same as that in Brown & Ahlers (2007) for the azimuthal temperature amplitude which was assumed to be instantaneously proportional to the LSC flow strength. However, the coefficients in τ_δ and δ_0 are slightly different from the 3D case due to the different geometries. Since $\delta = |\Delta_{bot}|$, the equation is invariant to the change of the flow directions, namely the sign of Δ_{bot} (see (3.4) below on how to map $\delta(t)$ back to the measured quantity $\Delta_{bot}(t)$).

The first two terms on the right-hand side represent respectively the buoyancy force and the viscous drag from the boundary layer. The stochastic driving term f_δ models the small-scale turbulent fluctuations and is assumed to be Gaussian distributed noise with zero mean. Equation (3.1) is motivated from the Navier–Stokes equation, which is only one of two governing equations for Rayleigh–Bénard convection. The other one is the heat transport equation $\dot{T} = -\boldsymbol{u}\cdot\boldsymbol{\nabla}T + \kappa\nabla^2 T$. In the quasi-2D system, the main LSC is diagonally oriented in the cell and the two small diagonally opposing corner rolls are occupied by the counter-rotating rolls (Sugiyama *et al.* 2010). Roughly speaking, the temperature difference across, and the velocity of, the corner rolls are of the same order as those of the main LSC roll. However, the corner rolls constantly damp the LSC because of their opposite flow directions. This may be modelled using the advective term in the heat transport equation, i.e. $-\boldsymbol{u}\cdot\boldsymbol{\nabla}T \sim -\nu Re\delta/H^2$. This term is proportional to δ, similar to the buoyancy term that describes the driving force of the LSC. This is because the corner rolls are also fed from buoyancy force through plume detachments from the boundary layers (Sugiyama *et al.* 2010). In the above, we have taken the size and velocity of the corners to be constant and have lumped their fluctuations into the stochastic term because their variations are affected by similar turbulent fluctuations. It should be noted that, due to the inertia of the growing corner

roll, the stochastic term $f_\delta(t)$ in our case could be a coloured noise instead of a white noise for a 3D system. This effect would make the system favour the reversal when δ is close to zero. However, detailed examination of these arguments is beyond the scope of this paper and should be tested in the future.

The other term in the heat equation is thermal diffusion, which has been assumed to contribute mostly in the thermal boundary layers (Brown & Ahlers 2008; Assaf *et al.* 2011). As the LSC is the self-organized flow of thermal plumes (Kadanoff 2001; Xi, Lam & Xia 2004), it is important to include thermal diffusion of plumes when considering the LSC dynamics. Thermal plumes may be viewed as consisting of a cap with a sharp temperature gradient over a distance close to the thermal boundary layer thickness. Therefore the thermal diffusion of plumes is of the order of $\kappa\nabla^2 T \approx \kappa(\Delta T/2)/\lambda_\theta^2$, where λ_θ is the thermal boundary layer thickness $\lambda_\theta = H/(2Nu)$. This term contributes in the fractional volume V_{pl}/V, with V_{pl} and V the volume of thermal plumes and that of the system respectively. The thickness of the thermal plumes is proportional to the thermal boundary layer thickness, so $V_{pl}/V = c' f_{pl}\lambda_\theta/H \times N_{pl}$, where N_{pl} is the total number of thermal plumes, f_{pl} is the surface area ratio between the plumes and the plate, and c' is a constant. It has been found experimentally that N_{pl} is related to Nu, i.e. $N_{pl} \sim Nu$, and $f_{pl} \sim Ra^{0.23}$ (Zhou & Xia 2010). The experiment by Zhou & Xia (2010) was conducted in three cells with different aspect ratios, and it was found that there is a positive relation between N_{pl} and Γ, but the exact relation is not known due to the limited choices of aspect ratio. Here, for simplicity, we assume that there is a power-law relation $N_{pl} \sim Nu\Gamma^\alpha$ with $\alpha > 0$. With the two extra terms from the heat transport equation added to (3.1), we have

$$\dot{\delta} = \frac{\delta}{\tau_\delta} - \frac{\delta^{3/2}}{\tau_\delta\sqrt{\delta_0}} - V_c\frac{\nu Re}{H^2}\delta + C\frac{\kappa\Delta T Nu^2 Ra^{0.23}}{H^2}\Gamma^\alpha + f_\delta(t), \tag{3.2}$$

where $V_c(\Gamma)$ and C are two prefactors that represent the geometrical coefficients from volume averaging, and C also contains the prefactor c' in the plume volume ratio V_{pl}/V. The equation represents a generic model that should apply to both 2D and 3D cases. We remark, however, that in addition to the corner roll term, the thermal diffusion term in the present model represents thermal diffusion in the bulk rather than in the boundary layers as in the previous 3D models (Brown & Ahlers 2008; Assaf *et al.* 2011), as thermal diffusion is bulk-dominated after volume averaging (He, Tong & Xia 2007).

We next simplify the model for the 2D case. The factor $V_c(\Gamma)$ controls the contribution of the corner roll relative to that of the LSC main roll and in principle depends on the aspect ratio. We set it as a constant for now as a first-order approximation, but will later make higher-order corrections using experimentally determined potential parameters. Based on experimental observations, we set the volume ratio between the corner roll and the main LSC roll to be 0.1. As the geometrical coefficient for the main LSC roll is 108 in the first term δ/τ_δ, this gives $V_c \approx 10.8$. For a median value of Ra in our parameter range, $\delta = 0.1$ K and $Re = 5000$, the damping force from the corner roll is thus $10.8\nu Re\delta/H^2 = 0.28$, which is much larger than the damping from the viscous boundary layer $\sqrt{54\alpha g}Re^{-1/4}\delta^{3/2}/H^{1/2} = 4\times10^{-3}$. This quantitative result is consistent with the previous observation that the growth of the corner roll is the main force that damps the LSC and leads to reversals (Sugiyama *et al.* 2010). Therefore the equation becomes a linear differential equation,

$$\dot{\delta} = -A\delta + B + f_\delta(t), \tag{3.3}$$

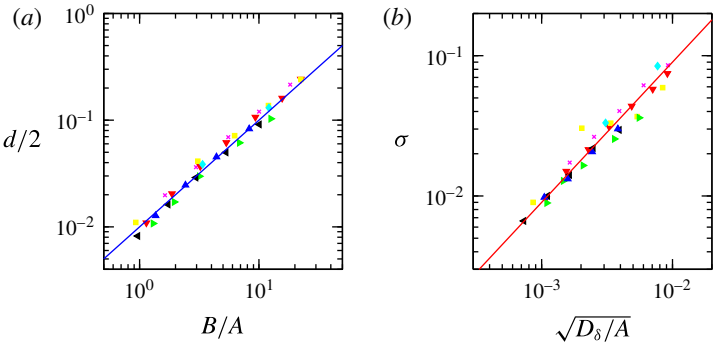

FIGURE 4. Comparison between experimental results and model predictions. The solid lines in both panels represent a linear relationship between the x and y axes, and all symbols are the same as in figure 3. (a) The separation $d/2$ between the two peaks in $p(\delta)$ versus the prediction from the model, B/A. (b) The variance σ of δ for each flow direction of the LSC versus the model prediction $\sqrt{D_\delta/A}$.

where $A = -1/\tau_\delta + 10.8\nu Re/H^2$ and $B = C\kappa\Delta TNu^2Ra^{0.23}\Gamma^\alpha/H^2$. To obtain the measurable quantity Δ_{bot}, we recall that $\delta = |\Delta_{bot}|$, thus Δ_{bot} can be numerically solved from

$$\Delta_{bot}(t) = \mathrm{sign}(\Delta_{bot}(t-\Delta t))[\delta(t-\Delta t) + \dot{\delta}(t-\Delta t)\Delta t]. \tag{3.4}$$

In contrast to $\delta(t)$, the quantity in the square brackets could become negative. When it does, it would switch the sign of Δ_{bot}, leading to a possible reversal event. Equations (3.3) and (3.4) combined together state that the motion of Δ_{bot} may be described by diffusion in two symmetrical harmonic potential wells driven by a stochastic force.

As $f_\delta(t)$ is a Gaussian distributed noise with zero mean, the diffusivity D_δ is used to describe the diffusion and can be determined from the experimental data. From the measured time series through $\langle[\delta(t+\mathrm{d}t) - \delta(t)]^2\rangle = D_\delta\,\mathrm{d}t$, we find that the non-dimensionalized diffusivity for different aspect ratios collapses onto one single power-law relation: $D_\delta(H^2/\Delta T^2\nu) \sim Ra^{0.43}$. Comparing with $\sim Ra^{-0.04}$ in the 3D case (Brown & Ahlers 2008), the Ra dependence of diffusivity in the quasi-2D case is much stronger.

The probability distribution $p(\delta)$ of the amplitude δ can be calculated from the steady-state solution of the Fokker–Planck equation corresponding to (3.3), which is $p(\delta) \sim \exp(-2V_\delta/D_\delta)$ with the parabolic potential well $V_\delta = A\delta^2/2 - B\delta$ (Gardiner 2004). Therefore $p(\delta)$ is a Gaussian function with variance $\sigma^2 = D_\delta/A$ and peak position at B/A. In figure 2 the experimentally measured $p(\delta)$ for each circulation state of the LSC is independently fitted with a Gaussian function, from which we obtain the variance σ and the peak position for each flow direction. It is found that σ is almost the same for the two peaks, but due to measurement uncertainties and imperfections in the experimental apparatus, the two peak positions in figure 2 are not exactly symmetric about zero. Therefore we use the separation d between the two peaks, which is roughly twice the peak position for each individual flow direction, for comparison with the model predicted position B/A. In both figures 4(a) and (b) the y axes are experimental results from the measured PDF and the x axes are the corresponding model predictions. The solid line shows a linear relation between

the x and y axes, which corresponds to the case that the model and experiments agree with each other. It is seen that nearly all symbols collapse with this solid line, indicating that our model captures the essential physics of the reversal process in a quasi-2D system. It should be noted that the exponent α in the constant term $B = C\kappa\Delta TNu^2Ra^{0.23}\Gamma^\alpha/H^2$ is not known in the model and it is determined here by minimizing experimental data scatter around the solid line in figure 4(*a*). This gives $\alpha = 4$. The coefficient C is set to be one in figure 4(*a*), as its value is not important in demonstrating the linear relationship between d and B/A.

Having calculated the complete $p(\delta)$, we can now extract the time interval between two successive reversals using the backward Fokker–Planck equation (Gardiner 2004), i.e.

$$\langle\tau\rangle/t_E = \frac{C_p}{t_E}\exp[2V_\delta(d/2)/D_\delta] = \frac{C_p}{t_E}\exp[-(d/2\sigma)^2], \tag{3.5}$$

where $C_p/t_E = \sqrt{2\pi D_\delta/A}/Bt_E = 2\sqrt{2\pi}\sigma^3/dD_\delta t_E$. In our parameter range, C_p/t_E is almost a constant, but the model prediction will be smaller than the experimental result because of the unsymmetrical PDF shown in figure 2. From figure 4 we see that there are small variations in the slope among different data sets. This is caused by setting $V_c(\Gamma)$ as a constant, since the two terms that make up the parameter A both have power-law dependences on Ra and thus give rise to a composite power law with an effective exponent. This effective exponent in fact varies over a small range, depending on the value of $V_c(\Gamma)$ (and hence Γ). Figure 4 shows that, to a first-order approximation, ignoring this variation works well for the purpose of testing the model prediction for the PDF $p(\delta)$. However, for $\langle\tau\rangle$ this will not be the case, as it has an exponential dependence on the harmonic potential. To make a high-order correction, we can fit a power law to the measured d and σ for each aspect ratio separately and then from them obtain the parameters A (and B) for the corresponding Γ. Operationally, we simply substitute A and B in the model potential with d and σ. The results are shown as the solid lines in figure 3. Here, C_p/t_E is chosen by shifting the solid lines vertically to match the symbols. It is seen that our model can describe the highly nonlinear and non-power-law dependence of $\langle\tau\rangle$ on Ra well, which again is an indication that our model correctly captures the essential features of the reversal dynamics in quasi-2D convection. It should be noted that the Ra dependence of $\langle\tau\rangle$ predicted by the model is stretched exponential, which is the strongest Ra dependence that has ever been observed. This will lead to extremely fast growth of $\langle\tau\rangle$ as Ra increases and explains why it is difficult to observe any reversals in the quasi-2D system when Ra becomes large (Sugiyama *et al.* 2010).

Finally, we comment on the relationship between the quasi-2D and 3D systems. It is known that corner rolls exist also in 3D systems (Sun *et al.* 2005). However, unlike the quasi-2D case, the corner rolls in 3D are not confined in the LSC plane. This means that, when fed with energy, the corner rolls do not need to grow in diameter, at the expense of shrinking the main LSC roll; rather, they can move or grow outside the LSC plane. Thus, the more generic corner roll term in (3.2) should be $-\nu V_c Re\delta/H^2 \times (\hat{\boldsymbol{u}}_c \cdot \hat{\boldsymbol{u}})$, where the two unit vectors $\hat{\boldsymbol{u}}_c$ and $\hat{\boldsymbol{u}}$ denote the directions of the velocities of the corner roll and the LSC. The extra term $(\hat{\boldsymbol{u}}_c \cdot \hat{\boldsymbol{u}})$ represents the projection of the corner roll contribution to the LSC plane. This term goes to one for a quasi-2D system. In a 3D system, previous models without consideration of the corner rolls work well for experimental results (Brown & Ahlers 2008; Assaf *et al.* 2011), which suggests that the corner roll effect in 3D is negligibly small compared with the viscous damping. This may suggest that the corner roll effect in a 3D system is most likely to influence motions perpendicular to the main LSC plane. For instance, its growth

pushes the LSC plane to rotate in the azimuthal direction and could be the origin of the azimuthal oscillation (Cioni *et al.* 1997; Brown *et al.* 2005; Sun *et al.* 2005; Xi *et al.* 2006).

Acknowledgements

We thank E. Brown for helpful discussions and the Hong Kong Research Grants Council (RGC) for support under grant nos CUHK 403712 and 404513.

References

AHLERS, G., GROSSMANN, S. & LOHSE, D. 2009 Heat transfer and large scale dynamics in turbulent Rayleigh–Bénard convection. *Rev. Mod. Phys.* **81**, 503–537.

ARAUJO, F. F., GROSSMANN, S. & LOHSE, D. 2005 Wind reversals in turbulent Rayleigh–Bénard convection. *Phys. Rev. Lett.* **95** (8), 084502.

ASSAF, M., ANGHELUTA, L. & GOLDENFELD, N. 2011 Rare fluctuations and large-scale circulation cessations in turbulent convection. *Phys. Rev. Lett.* **107**, 044502.

BENZI, R. 2005 Flow reversal in a simple dynamical model of turbulence. *Phys. Rev. Lett.* **95** (2), 024502.

BROWN, E. & AHLERS, G. 2006 Rotations and cessations of the large-scale circulation in turbulent Rayleigh–Bénard convection. *J. Fluid Mech.* **568**, 351–386.

BROWN, E. & AHLERS, G. 2007 Large-scale circulation model for turbulent Rayleigh–Bénard convection. *Phys. Rev. Lett.* **98** (13), 134501.

BROWN, E. & AHLERS, G. 2008 A model of diffusion in a potential well for the dynamics of the large-scale circulation in turbulent Rayleigh–Bénard convection. *Phys. Fluids* **20** (7), 075101.

BROWN, E., NIKOLAENKO, A. & AHLERS, G. 2005 Reorientation of the large-scale circulation in turbulent Rayleigh–Bénard convection. *Phys. Rev. Lett.* **95**, 084503.

CHANDRA, M. & VERMA, M. K. 2011 Dynamics and symmetries of flow reversals in turbulent convection. *Phys. Rev.* E **83** (6), 067303.

CHANDRA, M. & VERMA, M. K. 2013 Flow reversals in turbulent convection via vortex reconnections. *Phys. Rev. Lett.* **110** (11), 114503.

CHILLÀ, F. & SCHUMACHER, J. 2012 New perspectives in turbulent Rayleigh–Bénard convection. *Eur. Phys. J.* **35**, 58.

CIONI, S., CILIBERTO, S. & SOMMERIA, J. 1997 Strongly turbulent Rayleigh–Bénard convection in mercury: comparison with results at moderate Prandtl number. *J. Fluid Mech.* **335**, 111–140.

VAN DOORN, E., DHRUVA, B., SREENIVASAN, K. & CASSELLA, V. 2000 Statistics of wind direction and its increments. *Phys. Fluids* **12**, 1529–1534.

GARDINER, C. W. 2004 *Handbook of Stochastic Methods*. Springer.

GLATZMAIER, G. A., COE, R. S., HONGRE, L. & ROBERTS, P. H. 1999 The role of the Earth's mantle in controlling the frequency of geomagnetic reversals. *Nature* **401**, 885–890.

HE, X.-Z., TONG, P. & XIA, K.-Q. 2007 Measured thermal dissipation field in turbulent Rayleigh–Bénard convection. *Phys. Rev. Lett.* **98**, 144501.

KADANOFF, L. 2001 Turbulent heat flow: structures and scaling. *Phys. Today* **54** (8), 34.

LAM, S., SHANG, X.-D., ZHOU, S.-Q. & XIA, K.-Q. 2002 Prandtl number dependence of the viscous boundary layer and the Reynolds numbers in Rayleigh–Bénard convection. *Phys. Rev.* E **65**, 066306.

LOHSE, D. & XIA, K.-Q. 2010 Small-scale properties of turbulent Rayleigh–Bénard convection. *Annu. Rev. Fluid Mech.* **42**, 335–364.

SREENIVASAN, K. R., BERSHADSKII, A. & NIEMELA, J. J. 2002 Mean wind and its reversal in thermal convection. *Phys. Rev.* E **65**, 056306.

SUGIYAMA, K., NI, R., STEVENS, R. J. A. M., CHAN, T.-S., ZHOU, S.-Q., XI, H.-D., SUN, C., GROSSMANN, S., XIA, K.-Q. & LOHSE, D. 2010 Flow reversals in thermally driven turbulence. *Phys. Rev. Lett.* **105**, 034503.

SUN, C., XI, H.-D. & XIA, K.-Q. 2005 Azimuthal symmetry, flow dynamics, and heat transport in turbulent thermal convection in a cylinder with an aspect ratio of 0.5. *Phys. Rev. Lett.* **95**, 074502.

TSUJI, Y., MIZUNO, T., MASHIKO, T. & SANO, M. 2005 Mean wind in convective turbulence of mercury. *Phys. Rev. Lett.* **94** (3), 034501.

VASILEV, A., YU & FRICK, P. G. 2011 Reversals of large-scale circulation in turbulent convection in rectangular cavities. *JETP Lett.* **93**, 330–334.

WAGNER, S. & SHISHKINA, O. 2013 Aspect-ratio dependency of Rayleigh–Bénard convection in box-shaped containers. *Phys. Fluids* **25** (8), 085110.

XI, H.-D., LAM, S. & XIA, K.-Q. 2004 From laminar plumes to organized flows: the onset of large-scale circulation in turbulent thermal convection. *J. Fluid Mech.* **503**, 47–56.

XI, H.-D. & XIA, K.-Q. 2007 Cessations and reversals of the large-scale circulation in turbulent thermal convection. *Phys. Rev.* E **75** (6), 066307.

XI, H.-D., ZHOU, Q. & XIA, K.-Q. 2006 Azimuthal motion of the mean wind in turbulent thermal convection. *Phys. Rev.* E **73** (5), 056312.

XIA, K.-Q. 2013 Current trends and future directions in turbulent thermal convection. *Theor. Appl. Mech. Lett.* **3**, 052001.

XIA, K.-Q., SUN, C. & ZHOU, S.-Q. 2003 Particle image velocimetry measurement of the velocity field in turbulent thermal convection. *Phys. Rev.* E **68**, 066303.

XIA, K.-Q., ZHOU, S.-Q. & SUN, C. 2005 Statistics and scaling of the velocity field in turbulent thermal convection. In *Progress in Turbulence*, pp. 163–170.

YANAGISAWA, T., YAMAGISHI, Y., HAMANO, Y., TASAKA, Y. & TAKEDA, Y. 2011 Spontaneous flow reversals in Rayleigh–Bénard convection of a liquid metal. *Phys. Rev.* E **83** (3), 036307.

ZHOU, Q. & XIA, K.-Q. 2010 Physical and geometrical properties of thermal plumes in turbulent Rayleigh–Bénard convection. *New J. Phys.* **12**, 075006.